

A Novel Anti-tumor Cytokine Contains an RNA Binding Motif Present in Aminoacyl-tRNA Synthetases*

Received for publication, March 28, 2000, and in revised form, June 2, 2000
Published, JBC Papers in Press, June 13, 2000, DOI 10.1074/jbc.C000216200

Youngsoo Kim^{‡§}, Joongchul Shin[‡], Rongbao Li[¶], Chaejoon Cheong^{||}, Kyounghee Kim^{**},
and Sunghoon Kim^{**}

From the [‡]School of Chemical Engineering, Yeungnam University, 214-1 Dae-Dong, Kyungsan Kyungbuk 712-749, South Korea, the [¶]Department of Biological Structure, University of Washington, Seattle, Washington 98195, the ^{||}Magnetic Resonance Team, Korea Basic Science Institute, Eon-Dong Daejeon 305-333, South Korea, and the ^{**}National Creative Research Initiatives Center for ARS Network, Sung Kyun Kwan University, Chunchun-Dong, Suwon Kyunggido 440-746, South Korea

Endothelial monocyte-activating polypeptide II (EMAP II) is a novel pro-apoptotic cytokine that shares sequence homology with the C-terminal regions of several tRNA synthetases. Pro-EMAP II, the precursor of EMAP II, is associated with the multi-tRNA synthetase complex and facilitates aminoacylation activity. The structure of human EMAP II, solved at 1.8 Å resolution, revealed the oligomer-binding fold for binding different tRNAs and a domain that is structurally homologous to other chemokines. The similar structures to the RNA binding motif of EMAP II was previously observed in the anticodon binding domain of yeast Asp-tRNA synthetase (AspRSSC) and the B2 domain of *Thermus thermophilus* Phe-tRNA synthetase. The RNA binding pattern of EMAP II is likely to be nonspecific, in contrast to the AspRSSC. The peptide sequence that is responsible for cytokine activity is located, for the most part, in the β1 strand. It is divided into two regions by a neighboring loop.

Endothelial monocyte-activating polypeptide II (EMAP II)¹ is a novel cytokine that was first isolated from a methylcholanthrene A-transformed fibrosarcoma. However, it is expressed in normal cells and is involved in apoptosis during development (1). The functional cytokine domain (EMAP II) is located in the C-terminal 166 amino acids of its precursor (pro-EMAP II) and is released by proteolysis (2). Recently, caspase-7 was identified as responsible for the proteolytic mat-

uration of pro-EMAP II, thereby linking apoptosis to inflammation (3). Pro-EMAP II, previously known also as p43, is associated with the multi-tRNA synthetase complex in higher eukaryotes (4).

The N-terminal domain of pro-EMAP II containing 146 amino acids does not show homology to any known proteins and interacts with the N-terminal extension of human arginyl-tRNA synthetase. In contrast, the C-terminal domain of pro-EMAP II can interact with different tRNAs. The interaction with pro-EMAP II stimulated aminoacylation activity of the bound arginyl-tRNA synthetase, but its separated N- or C-terminal domain alone did not (5). This result suggested that pro-EMAP II delivers the tRNA, which is bound to the C-terminal domain, to the active site of the associated tRNA synthetase. Interestingly, despite the cytokine activity of the EMAP II, it is not homologous to any known cytokine in the amino acid sequence. It is homologous, however, to the C-terminal regions of methionyl-tRNA synthetases of prokaryotes, archaeas, and nematodes (4), human tyrosyl-tRNA synthetase (6), and yeast Arc1p (7), which is associated with other tRNA synthetases. Although its homology to the domains of various tRNA synthetases appears to be responsible for its ability to bind tRNA, the property of tRNA binding is not structurally explained.

Although pro-EMAP II facilitates protein synthesis by its stimulatory effect on the catalytic activity of the associated tRNA synthetases, its proteolytic product, EMAP II, accelerates apoptosis, suggesting its dual function in cell viability and death. A similar phenomenon was also reported in the case of human tyrosyl-tRNA synthetase, which is secreted from serum-starved cells and cleaved into two distinct cytokines (8). The N- and C-terminal domains of this enzyme showed interleukin-8- and EMAP II-like functions, respectively.

Although the EMAP II-like domain is widely distributed among different tRNA synthetases and their association factors (such as p43, Arc1p, and Trbp111 (9) isolated from various species), the structural information of this domain is limited. In particular, the lack of structural information on EMAP II makes it difficult to understand its diverse biological activities and maturation process. In this report, we discuss the x-ray structure of human EMAP II solved at 1.8 Å resolution as well as the structural features of the oligomer-binding fold (OB fold) (10) for binding different tRNAs and peptide sequences for cytokine activities.

EXPERIMENTAL PROCEDURES

Purification of EMAP II—The human EMAP II gene was cloned into a pET28a vector as described previously (5), except that two restriction

* This work was supported by Grant 99-N1-06-01-A-06 from the Ministry of Science and Technology Biotech 2000 program (to Y. K.) and also in part by a grant from the National Creative Research Initiatives of the Ministry of Science and Technology (to S. K.). The costs of publication of this article were defrayed in part by the payment of page charges. This article must therefore be marked "advertisement" in accordance with 18 USC Section 1734 solely to indicate this fact.

The atomic coordinates for EMAP II (code 1euj) have been deposited in the Protein Data Bank, Research Collaboratory for Structural Bioinformatics, Rutgers University, New Brunswick, NJ (<http://www.rcsb.org/>).

§ To whom correspondence should be addressed: University of Washington, Health Sciences Bldg. K-428, Box 357742, Seattle, WA 98195-7742. Tel.: 206-616-4292; Fax: 206-685-7002; E-mail: ykim1@u.washington.edu.

¹ The abbreviations used are: EMAP II, endothelial monocyte-activating polypeptide II; pro-EMAP II, precursor of EMAP II; AspRS, Asp-tRNA synthetase; AspRSSC, yeast Asp-tRNA synthetase; OB fold, oligonucleotide/oligosaccharide (or oligomer)-binding fold; PheRS, phenylalanyl-tRNA synthetase; PheRSTT, *Thermus thermophilus* phenylalanyl-tRNA synthetase; RANTES, regulated on activation normal T cell expressed; MES, 4-morpholineethanesulfonic acid; CM, carboxymethyl.

TABLE I
 Summary of crystallographic data

Values within parentheses are for the last shell of data.

	Native	CH ₃ HgCl
Diffraction data statistics		
Space group	C ₂	C ₂
Resolution	20 – 1.8 (1.89–1.80) Å	20 – 2.1 (2.21–2.10) Å
Overall observations	96,335	48,451
Unique observations	31,502	20,817
Completeness (%)	88.2 (37.9)	91.9 (85.2)
R _{merge} (%) ^a	6.8 (28.2)	6.2 (26.0)
$\langle I/\sigma I \rangle$	31.3 (1.8)	20.6 (2.3)
Lattice constants: $a = 134.01$ Å, $b = 38.34$ Å, $c = 80.99$ Å, $\alpha = \gamma = 90^\circ$, $\beta = 112.90^\circ$		
Phasing statistics		
Heavy atom sites		6
Phasing power ^b (acentrics/centrics)		2.13/1.79
R _{cullis} ^c (acentrics/centrics)		0.64/0.66
Refinement statistics		
Resolution	20 – 1.80 Å	
No. of reflections	30,839	
No. of reflections (R _{free} calculation)	2,329	
R _{cryst} ^d	20.8	
R _{free} ^e	23.2	
No. of non-hydrogen atoms		
Protein	2,510	
Water	193	
r.m.s.d. ^f		
Bonds (Å)	0.006	
Angles (°)	1.58	
Average B-factors	31.7	
Ramachandran analysis		
Most favored	88.4%	
Additionally favored	11.6%	

^a $R_{\text{sym}} = \sum |I - \langle I \rangle| / \sum I$.

^b Phasing power = (r.m.s. F_h)/(r.m.s. E), where F_h is the heavy atom structure amplitude and E is the residual lack of closure error.

^c $R_{\text{cullis}} = \sum |E| / \sum |\Delta F|$, where phasing power and R_{cullis} values were determined by SHARP¹⁴.

^d $R_{\text{cryst}} = \sum |F_{\text{obs}}| - |F_{\text{calc}}| / \sum |F_{\text{obs}}|$.

^e $R_{\text{free}} = \sum |F_{\text{obs}}| - |F_{\text{calc}}| / \sum |F_{\text{obs}}|$, where F_{obs} are test set amplitudes (2,329 reflections) not used in refinement.

^f r.m.s.d., root-mean-square deviations.

sites, *NcoI* and *SalI*, were used to remove the His tag.² EMAP II was expressed in *Escherichia coli* BL21(DE3) harboring pET28a-EMAP II. The cells were grown at 37 °C in an LB-kanamycin (30 µg/ml) broth with 1 mM isopropyl-1-thio-β-galactopyranoside to the cell density corresponding to 0.5 of A₆₀₀. Cells were harvested by centrifugation (6000 × *g* for 5 min), resuspended in an extraction buffer (20 mM MES, pH 5.5, 1 mM EDTA, 1 mM β-mercaptoethanol, 50 mM KCl, 0.5% Tween 20, 0.5% Nonidet P-40, and 50 mM glucose), and lysed by sonication. After centrifugation at 10000 × *g* for 15 min, the lysate was loaded on a CM-Sepharose ion exchange column, which was equilibrated with CM buffer (20 mM MES, pH 5.5, 1 mM EDTA, 1 mM β-mercaptoethanol). The proteins bound to the column were eluted by a five-column volume linear gradient of NaCl from 0 to 1000 mM in CM buffer. Fractions containing EMAP II were pooled, concentrated to 5 ml, and loaded on a Sephadex G-75 gel filtration column, which was equilibrated with a G-75 buffer (20 mM Tris-HCl, pH 8.0, 1 mM β-mercaptoethanol, 1 mM EDTA, and 100 mM KCl). EMAP II, eluted from a gel filtration column, was pooled and concentrated to 10 mg/ml for crystallization. When the 10 µg of purified EMAP II was loaded on a SDS-polyacrylamide gel no other bands were detected by Coomassie Brilliant Blue staining.

Crystallization and Data Collection—EMAP II was stored at 10 mg/ml in 20 mM Tris-HCl, pH 8.0, 0.5 mM β-mercaptoethanol, 1 mM EDTA, and 100 mM KCl. The crystals of EMAP II were grown over a period of 3 days at 21 °C in hanging drops formed by mixing 3 µl of the protein solution and 3 µl of a reservoir solution, which consisted of 100 mM sodium acetate, pH 4.6, 20% (w/v) polyethylene glycol 4000, and 15 mM MgCl₂. Cell dimensions are: $a = 134.01$ Å, $b = 38.34$ Å, $c = 80.99$ Å, $\alpha = \gamma = 90^\circ$, and $\beta = 112.90^\circ$. Crystal contains 2 molecules/asymmetric unit and 64% solvent. These crystals have a non-crystallographic 2-fold symmetry at $\omega = 36.7^\circ$, $\phi = 286.4^\circ$ and $\kappa = 180^\circ$, described in POLRFN (11). Native and heavy atom derivative data were collected at room temperature on a RAXIS IV detector with a Rigaku RU200 rotating anode (Cu-Kα) x-ray generator operated at 50 kV and 100 mA. All data were processed with DENZO and SCALEPACK (12).

Structure Determination—For heavy atom derivative analysis, the initial 6 mercury sites of CH₃HgCl were determined using SOLVE (13). Heavy atom parameters were refined using SHARP (14). A high quality electron density map was obtained using single isomorphous replacement phases. The map was further improved by density modification with SOLOMON (15). The phases were calculated to 2.1 Å using SHARP (14) and then extended to 1.8 Å using solvent flipping (15). Using O (16), the electron density map was readily traceable through the whole molecule, even to side chains without any ambiguous regions (Fig. 1, A and B). Thus, 2-fold non-crystallographic symmetry averaging was not needed to improve the electron density map. The EMAP II model includes residues 3–166 for each molecule in the asymmetric unit. The 2 residues in the N terminus were disordered, and the third residue is registered as Ala.

All crystallographic refinements were carried out using CNS (17) with maximum likelihood refinement, bulk solvent correction, and corrections for anisotropic diffraction. Ramachandran plot analysis with PROCHECK (18) showed that all residues in the current model are in the most favorable and additionally allowed regions. Data phasing and refinement statistics are shown in Table I. Figures were generated with the programs Molscript (19), Bobscrip (20), and Raster3D (21).

RESULTS AND DISCUSSION

Overall Structure—The crystal structure of EMAP II was solved using the single isomorphous replacement method (Table I). The final model contains two molecules per asymmetric unit (residues 3–166, respectively) and 193 water molecules refined at 1.8 Å resolution (Fig. 1, A–C). The EMAP II structure consists of 11 β-strands forming a structural core and three flanking α-helices (Fig. 1C): the strands β1 (residues 10–21), β2 (residues 28–34), β3 (residues 40–46), β4 (residues 59–66), β5i (residues 70–72), β6i (residues 75–77), β7 (residues 79–85), β8 (residues 90–92), β9 (residues 103–106), β10 (residues 132–134), β11 (residues 140–142), and the α-helices α1 (residues 53–56), α2 (residues 119–123), α3 (residues 124–130).

² S. Kim, unpublished data.

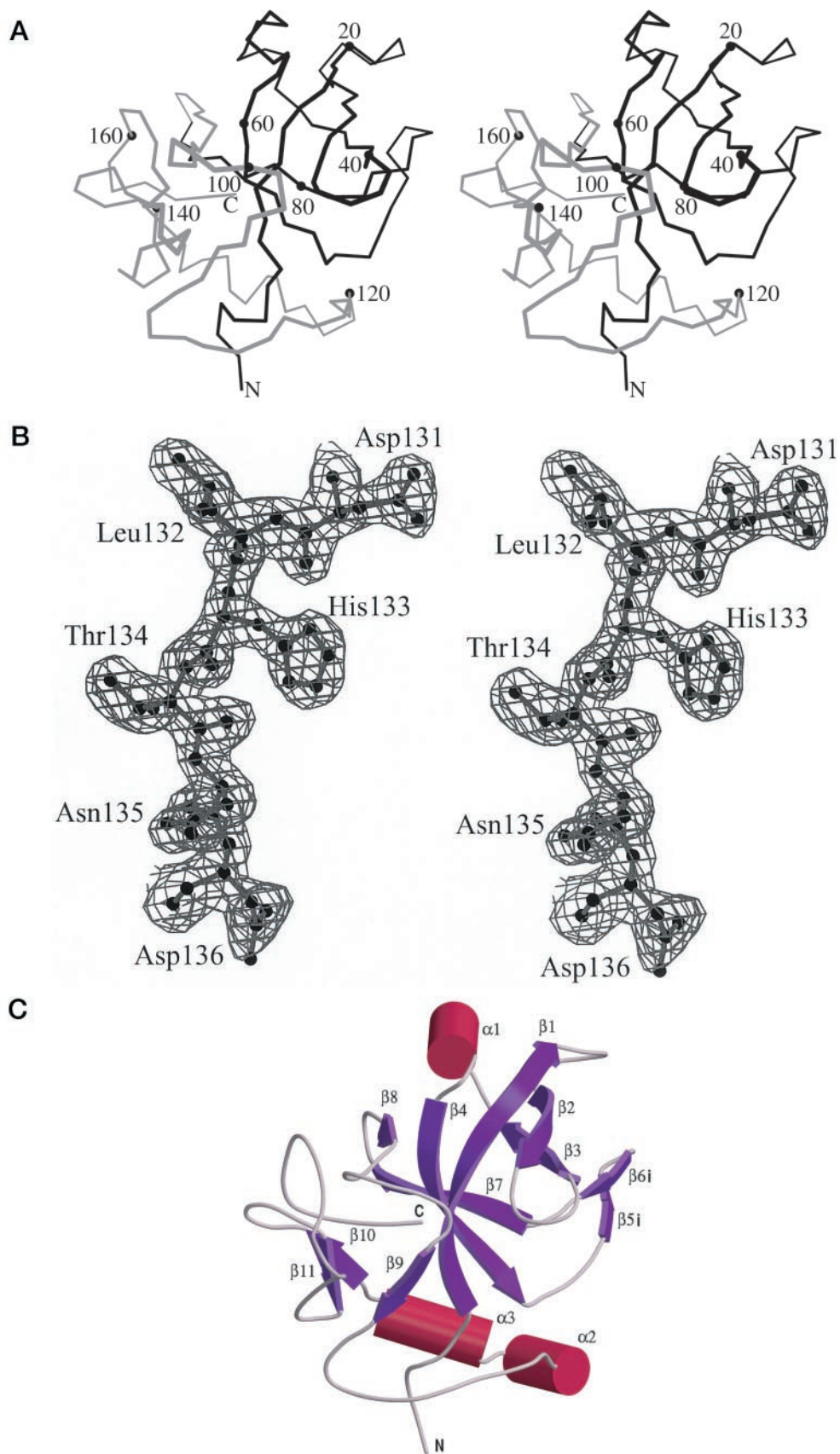


FIG. 1. Overall structure and experimental electron density map of EMAP II. *A*, stereo view of the EMAP II structure in a $C\alpha$ trace. The N-terminal region shows the OB fold in black and the loop-rich C-terminal region in gray. *N* represents the location of Pro-3 and *C* indicates the C terminus. Every 20th $C\alpha$ is labeled with a dark circle. *B*, stereo view of the experimental electron density map. The map calculated after solvent flipping is contoured at 1.2σ . The electron density map is superimposed upon refined coordinates of residues 131–136. Three residues (Asp-108, His-133, and Asp-136) of one molecule from the non-crystallographic 2-fold symmetry in the asymmetric unit are directly hydrogen-bonded to

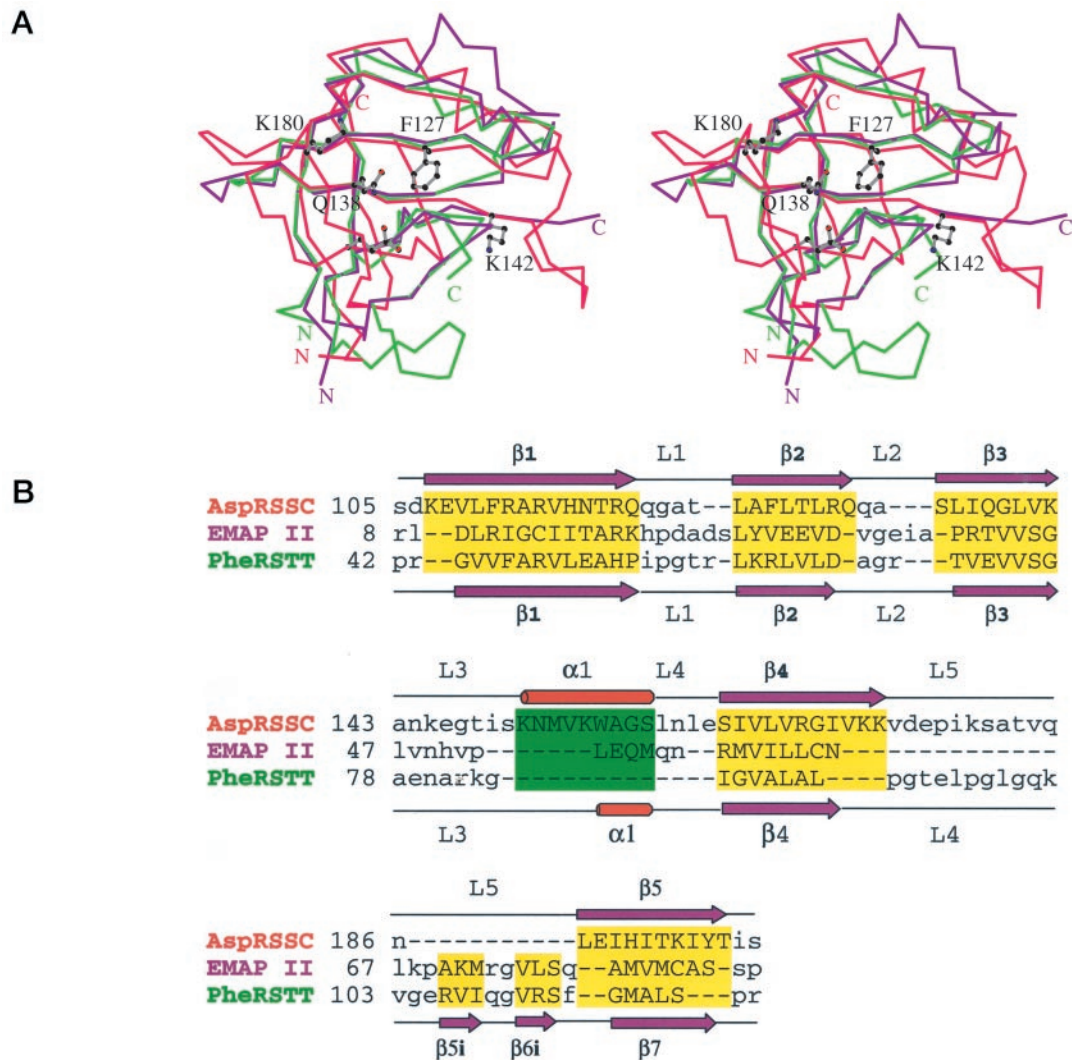


FIG. 2. Structural comparison of OB folds in AspRSSC (23), EMAP II, and PheRSTT (28). A, superposition of OB folds in AspRSSC, EMAP II, and PheRSTT. Stereo view of the three OB folds are shown as α traces. The anticodon binding domain of AspRSSC (red) is used as a reference, and five residues involved in specific interactions for anticodon bases (Phe-127, Gln-138, Lys-142, Lys-180, and Glu-188) are shown by ball-and-stick symbols to identify the binding sites. The residue Glu-188 is not labeled for a clear view. EMAP II is shown in purple and PheRSTT in green. The letters *N* represent the locations of Ser-105, Arg-8, and Pro-42 for AspRSSC, EMAP II, and PheRSTT, respectively. The letters *C* indicate the locations of Ser-198, Pro-87, and Arg-121 for AspRSSC, EMAP II, and PheRSTT, respectively. B, structure-based sequence alignment of the OB folds in AspRSSC (23), EMAP II, and PheRSTT (28). The nomenclature of the secondary structure elements is based on the same convention with a minor variation as described for the OB fold (10). The nomenclature of EMAP II is the same as in Fig. 1C. The locations of the secondary structure elements are indicated above and below the aligned sequences. The yellow boxes represent β -strands, and the green box represents α -helix. If there are no corresponding residues in the sequences, they are marked with a “-.” The secondary structure elements of AspRSSC are marked on the top, and those of EMAP II and PheRSTT follow the notation at the bottom. EMAP II and PheRSTT have some variations in the assignments of secondary structure elements compared with AspRSSC. For instance, PheRSTT lacks the helix $\alpha 1$, and both EMAP II and PheRSTT have two inserted short strands ($\beta 5i$ and $\beta 6i$). Therefore, the notations were changed accordingly. The residue numbers for each sequence are shown at the beginning of the sequence. The uppercase letters represent secondary structure elements, and the lowercase letters represent loop regions between the secondary structure elements. The arrows refer to β -strands and the cylinder to α -helix.

The structure can be divided into the N- and C-terminal regions. The N-terminal region, consisting of the strands $\beta 1$ –7 and the helix $\alpha 1$, forms a distinct structural motif called the OB fold (10), which is known to bind oligonucleotide and oligosaccharide. The OB fold of EMAP II has a five-stranded Greek key β -barrel (strands $\beta 1$ –3, $\beta 4$, and $\beta 7$) that is capped by the short helix $\alpha 1$, located between strands $\beta 3$ and $\beta 4$. The C-terminal region contains strands $\beta 8$ –11, helices $\alpha 2$ –3, and several long

loops. This C-terminal region contains longer loops than the N-terminal region. This region does not share homology with any known structure.

In the crystals, the two molecules exist in an asymmetric unit forming non-crystallographic, 2-fold symmetry. The two EMAP II in the asymmetric unit sit adjacent to each other, making contact at their interfacial surfaces. The two molecules contact weakly at the surfaces of the loops in the C-terminal

His-133, Asp-108, and Lys-150 of the other molecule, respectively. Only those two residues, His-133 and Asp-136, are shown in this typical region of experimental electron density map. C, secondary structure nomenclature to identify β -strands and α -helices. The α -helices are colored red, the β -strands purple, and the loops gray. Strands $\beta 5i$ and $\beta 6i$ are two short β -strands inserted in a region corresponding to loop L5 of AspRSSC (also see Fig. 2A).

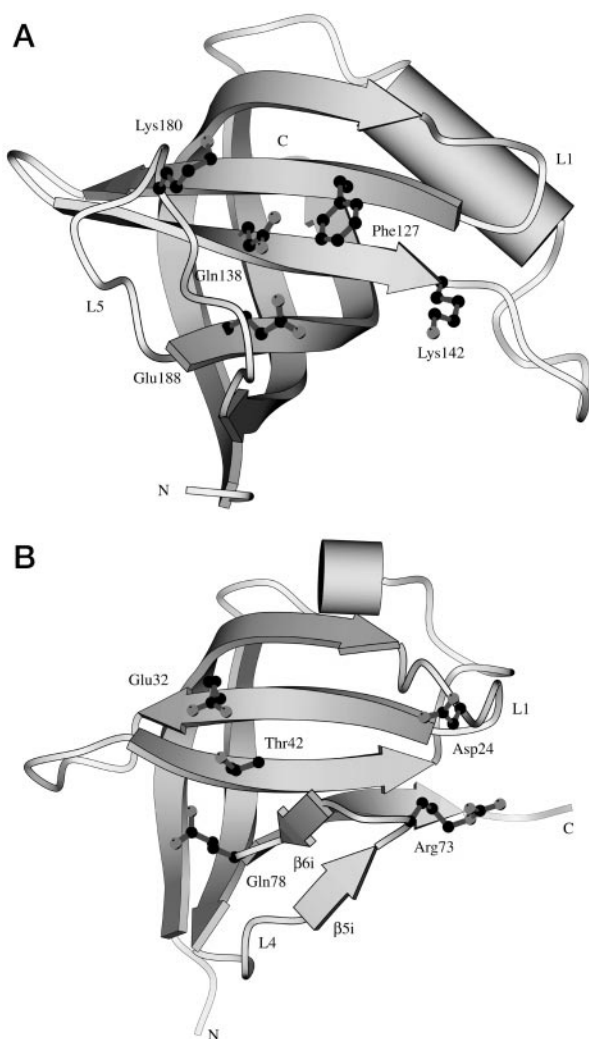


FIG. 3. Comparison of RNA binding motifs in the OB folds of EMAP II and AsprSSC (23) structures. The orientations and residues are the same as described for Fig. 2A. The nomenclature of secondary structure elements follows the same convention as used in Figs. 1C and 2B. A, anticodon binding motif of AsprSSC. The 5 residues are shown to interact specifically with the three anticodon bases of Asp-tRNA by hydrogen bonds. Loop L5 is oriented so that it forms a valley to generate the binding pocket for the anticodon bases of Asp-tRNA. N represents the location of Ser-105 and C the location of Ser-198. B, RNA binding motif of EMAP II. The probable candidate residues, which may interact with tRNAs nonspecifically, are inferred from a comparison of the conserved residues in the EMAP II-like domains (4) with those involved in anticodon base interactions in the AsprSSC structure (23). The 5 hydrophilic residues are positioned in the smooth surface formed by loop L4, the strands $\beta 5i$ and $\beta 6i$ headed to the C terminus, whereas the residues of AsprSSC form a valley for the binding pocket of anticodon bases. N represents the location of Arg-8 and C the location of Pro-87.

region by three hydrogen bonds of residues 108, 133, and 136 (Fig. 1B). These surface contacts occur at the opposite end of EMAP II from the putative tRNA binding and cytokine activity sites and will be discussed later. Interestingly, a structure-specific tRNA-binding protein (Trbp111) from *Aquifex aeolicus* (9) and the C-terminal domain of *E. coli* methionyl-tRNA synthetase (data not shown),² which share sequence homologies with the OB fold of EMAP II, form dimers. However, the C-terminal region of EMAP II, which is involved in the dimer contacts in the asymmetric unit of the crystal, is not present in Trbp111 and the C-terminal domain of *E. coli* methionyl-tRNA synthetase (9). In addition, a gel filtration analysis showed that hamster EMAP II exists as a monomer in the solution (4). This

result was also confirmed by a two-hybrid assay (data not shown).² Although the dimer formation of EMAP II was observed in the gel shift assay using tRNA as a substrate, it occurred only at an extremely high concentration (500 μM) of EMAP II (4). Therefore, the active form of EMAP II at physiological condition is likely to be a monomer.

The tRNA Binding Domain of EMAP II—The architectures of many proteins are based on closed β -barrels, such as the OB fold, as described in the N-terminal region of EMAP II. The OB fold was first recognized as a common structural motif among four proteins: staphylococcal nuclease (22), aspartyl-tRNA synthetase (AspRS) (23), and the B-subunits of cholera-like (24) and shiga-like cytotoxins (25) from *E. coli*. Since then, 14 proteins have been identified as having the OB fold. Among the aminoacyl-tRNA synthetases, aspartyl- (23), lysyl- (26), asparaginyl- (27), and phenylalanyl-tRNA (28) synthetases (PheRS) contain the OB fold. In the first three tRNA synthetases, the OB fold is located in the N-terminal domain of about 90 residues and has been shown to be responsible for specific recognition of the anticodon loop of tRNA. In the PheRS, the OB fold is present in the B2 domain, whose function is not known (28). The OB folds from the yeast AspRS (AsprSSC), EMAP II, and *Thermus thermophilus* PheRS (PheRSTT) structures are aligned in the $C\alpha$ backbone (Fig. 2A), and their corresponding residues in the structural alignment can be identified (Fig. 2B). The OB fold for the AsprSSC structure is superimposed onto that of the EMAP II structure at 1.69 Å for 41 $C\alpha$ atoms, whereas the PheRSTT is at 1.18 Å for 66 atoms. The structural alignments show that the β -barrel of AsprSSC is closed between strands $\beta 3$ and $\beta 5$, whereas the corresponding β -barrels of EMAP II and PheRSTT ($\beta 3$ and $\beta 7$) are partially open (Fig. 2, A and B). The alignments also show that the helix $\alpha 1$ and loop L5 regions of AsprSSC are the least conserved among the three structures. EMAP II has a shorter $\alpha 1$ helix consisting of 4 residues, whereas AsprSSC has 9 residues in this helix. In contrast, the PheRSTT structure does not carry the α -helix. In addition, EMAP II and PheRSTT have two inserted short β -strands ($\beta 5i$ and $\beta 6i$) in the region corresponding to loop L5 of AsprSSC.

Gel mobility shift assays indicate that EMAP II can bind several tRNA species with similar dissociation constants (4). The OB fold of EMAP II is most likely to be responsible for this nonspecific tRNA binding. In the structure of AsprSSC that is complexed with tRNA (23), anticodon bases are bound to a valley formed on one side of the barrel. Residues from strands $\beta 1$, $\beta 2$, $\beta 3$, and $\beta 5$ form the floor of the valley, whereas residues from loops L1 and L5 line the edges. Specific interactions are formed from the conserved residues Phe-127, which stacks against the anticodon base U35, and both Gln-138 and Glu-188, which form hydrogen bonds to the anticodon bases (Figs. 2A and 3A). If we assume that a tRNA approaches the OB fold from the same direction in both AspRS and EMAP II, then their binding patterns would be somewhat different. In EMAP II, the close proximity of loops L1, L4, $\beta 5i$, and $\beta 6i$ provides a smooth surface for the interaction with the incoming tRNA instead of a specific binding pocket of AsprSSC (Figs. 2A and 3B). For example, there are no aromatic side chains exposed on the side of the β -barrel, as found in Phe-127 of AsprSSC. Instead, several residues, such as Asp-24, Glu-32, Thr-42, Arg-73, and Gln-78, are exposed to solvent. These 5 residues are highly conserved among the proteins with the EMAP II-like domain (4, 9). Thus, the nonspecificity in the tRNA binding of the EMAP II-like domain is likely to occur through these residues on the surface. The structural similarity between the OB fold of EMAP II and the B2 domain of PheRSTT probably predicts that the B2 domain may also function as a nonspecific binder of

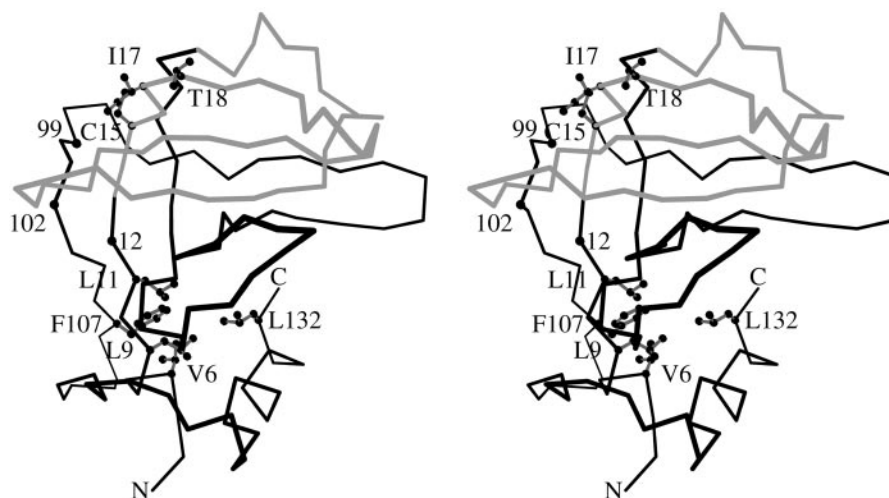


FIG. 4. **Domain with cytokine activity.** Stereo views of EMAP II are shown as Ca traces, truncated at residue 133 for a clear view. The view is in the same orientation as Fig. 3B. The domain, consisting of the residues 13–57, which is homologous to the chemokines, is shown in gray and consists of three strands (β 1– β 3) and one short helix (α 1). The peptide sequence (residues 12–18) involved in chemotaxis of EMAP II is positioned at the beginning of this homologous domain. Three residues, Cys-15, Ile-17, and Thr-18, which were exposed to solvent, are shown by ball-and-stick symbols close to the end of strand β 1. The other functional peptide sequence (residues 6–11) is located at the other side of a loop formed by residues 99–102. The hydrophobic residues Val-6, Leu-8, and Leu-11 form a shallow hydrophobic pocket with Phe-107 and Leu-132. N represents the location of Pro-3 and C the location of His-133. The Cas of residues 12, 99, and 102 are shown as black circles.

tRNAs. Presumably, all of the proteins containing the EMAP II-like domain will carry the partially open OB fold that is shown in the EMAP II and PheRSTT structures. This may provide a capability to function as a nonspecific binder of tRNAs.

Implications for Cytokine Function—The structural homology search program DALI (29) identified that the N-terminal 45 residues of EMAP II (residues 13 to 57) have limited structural homologies with monomers of chemokines, such as RANTES (residues 22–61) (30), human monocyte chemoattractant protein (residues 25–65) (31), and neutrophil-activating peptide-2 (residues 38–79) (32). They share a similar structural motif consisting of a three-stranded β -sheet with an α -helix. In EMAP II, strands β 1– β 3 and helix α 1 form a homologous structural domain of monomers of these chemokines (Fig. 4) even though the primary sequence of EMAP II shows no homology. The Cas of those chemokine structural motifs in RANTES, human monocyte chemoattractant protein, and neutrophil-activating peptide-2 could be superimposed onto the corresponding region of EMAP II with root-mean-square deviations of 1.78, 1.75, and 2.5 Å for 30, 23, and 21 atoms, respectively.

Studies on murine and human EMAP II (33, 34) suggest that the residues responsible for cytokine activity in human EMAP II are the residues from 6 to 18 (VSRLDLRIGCIIT). This peptide stimulated chemotaxis and increased cytosolic calcium in mononuclear phagocytes and polymorphonuclear leukocytes, whereas the last 7 residues (residues 12–18, RIGCIIT) trigger only chemotaxis. The 13 residues for those cytokine activities lie mostly in a long stretch of strand β 1 (Fig. 4). The Val-6, Leu-9, and Leu-11 form a shallow hydrophobic pocket with neighboring residues, such as Phe-107 and Leu-132, in the solvent accessible surface. A short α -helix turn starts at residue Val-6. Residues 12–18, which mediate chemotaxis, are positioned toward the end of strand β 1, which is flanked by strands β 2 and β 4. Interestingly, these last 7 residues are separated from the first 6 residues by a loop consisting of residues 99–102. Three residues, Arg-12 to Gly-14, in the shorter sequence (RIGCIIT) are covered by the loop and only 3 residues (Cys-15, Ile-17, Thr-18) expose their side chains to solvent. Peptides with substitutions on position 18 had no cytokine activities (34). This may imply that residue Thr-18 plays a crucial role in

accessibility for receptor binding or other interactions for cytokine activity.

The ancient forms of aminoacyl-tRNA synthetase are thought to consist of the catalytic domain, which recognizes the minimalist acceptor stem of RNA for aminoacylation (35). During functional diversification, aminoacyl-tRNA synthetases might have adopted non-conserved RNA binding domains in *cis* or in *trans* to enhance catalytic efficiency or substrate specificity. Although the C-terminal extension of *E. coli* methionyl-tRNA synthetase (36) or the N-terminal extension of yeast glutamyl-tRNA synthetase (37) are cases of the *cis*-acting domain, Trbp111 of *A. aeolicus* (9) or mammalian EMAP II would be examples of *trans*-acting factors. In the mammalian system, in which cell growth and death are tightly controlled, EMAP II might have acquired an additional function as a cytokine so that it can functionally coordinate protein synthesis and programmed cell death.

Acknowledgments—We thank S.-E. Ryu for a gift of CH_3HgCl and M. Feese and M. Robien for critical reading of the manuscript. We acknowledge that the x-ray data were collected at the Yeungnam University Instrumental Analysis Center.

REFERENCES

1. Tas, M. P., and Murray, J. C. (1996) *Int. J. Biochem. Cell Biol.* **28**, 837–841
2. Knies, U. E., Behrendorf, H. A., Mitchell, C. A., Deutsch, U., Risau, W., Drexler, H. C., and Clauss, M. (1998) *Proc. Natl. Acad. Sci. U. S. A.* **95**, 12322–12327
3. Behrendorf, H. A., van de Craen, M., Knies, U. E., Vandenabeele, P., and Clauss, M. (2000) *FEBS Lett.* **466**, 143–147
4. Quevillon, S., Agou, F., Robinson, J. C., and Mirande, M. (1997) *J. Biol. Chem.* **272**, 32573–32579
5. Park, S. G., Jung, K. H., Lee, J. S., Jo, Y. J., Motegi, H., Kim, S., and Shiba, K. (1999) *J. Biol. Chem.* **274**, 16673–16676
6. Kleeman, T. A., Wei, D., Simpson, K. L., and First, E. A. (1997) *J. Biol. Chem.* **272**, 14420–14425
7. Simos, G., Segref, A., Fasiolo, F., Hellmuth, K., Shevchenko, A., Mann, M., and Hurt, E. C. (1996) *EMBO J.* **15**, 5437–5448
8. Wakasugi, K., and Schimmel, P. (1999) *Science* **284**, 147–151
9. Morales, A. J., Swairjo, M. A., and Schimmel, P. (1999) *EMBO J.* **18**, 3475–3483
10. Murzin, A. G. (1993) *EMBO J.* **12**, 861–867
11. Collaborative Computational Project Number 4 (1994) *Acta Crystallogr. Sect. D Biol. Crystallogr.* **D50**, 760–763
12. Otwinowski, Z., and Minor, W. (1997) *Methods Enzymol.* **276**, 307–326
13. Terwilliger, T. C., and Berendzen, J. (1999) *Acta Crystallogr. Sect. D Biol. Crystallogr.* **D55**, 849–861
14. de La Fortelle, E., and Bricogne, G. (1996) *Methods Enzymol.* **276**, 472–494
15. Abrahams, J. P., and Leslie, A. G. W. (1996) *Acta Crystallogr. Sect. D Biol. Crystallogr.* **D52**, 30–42
16. Jones, T. A., Zhou, J.-Y., Cowan, S. W., and Kjeldgaard, M. (1991) *Acta*

- Crystallogr. Sect. A* **A47**, 110–119
17. Brunger, A. T., Adams, P. D., Clore, G. M., DeLano, W. L., Gros, P., Grosse-Kunstleve, R. W., Jiang, J. S., Kuszewski, J., Nilges, M., Pannu, N. S., Read, R. J., Rice, L. M., Simonson, T., and Warren, G. L. (1998) *Acta Crystallogr. Sect. D Biol. Crystallogr.* **D54**, 905–921
 18. Laskowski, R. A., MacArthur, M. W., Moss, D. S., and Thornton, J. M. (1993) *J. Appl. Crystallogr.* **26**, 283–291
 19. Kraulis, P. J. (1991) *J. Appl. Crystallogr.* **24**, 946–950
 20. Esnouf, R. M. (1997) *J. Mol. Graph.* **15**, 132–134
 21. Merritt, E. A., Bacon, D. J. (1997) *Methods Enzymol.* **277**, 505–524
 22. Hynes, T. R., and Fox, R. O. (1991) *Proteins* **10**, 92–105
 23. Ruff, M., Krishnaswamy, S., Boeglin, M., Poterszman, A., Mitschler, A., Podjarny, A., Rees, B., Thierry, J. C., and Moras, D. (1991) *Science* **252**, 1682–1689
 24. Sixma, T. K., Pronk, S. E., Kalk, K. H., Wartna, E. S., van Zanten, B. A., Witholt, B., and Hol, W. G. (1991) *Nature* **351**, 371–377
 25. Stein, P. E., Boodhoo, A., Tyrrell, G. J., Brunton, J. L., and Read, R. J. (1992) *Nature* **355**, 748–750
 26. Cusack, S., Yaremchuk, A., and Tukalo, M. (1996) *EMBO J.* **15**, 6321–6334
 27. Cusack, S., Hartlein, M., and Leberman, R. (1991) *Nucleic Acids Res.* **19**, 3489–3498
 28. Goldgur, Y., Mosyak, L., Reshetnikova, L., Ankilova, V., Lavrik, O., Khodyreva, S., and Safro, M. (1997) *Structure* **5**, 59–68
 29. Holm, L., and Sander, C. (1993) *J. Mol. Biol.* **233**, 123–138
 30. Wilken, J., Hoover, D., Thompson, D. A., Barlow, P. N., McSparron, H., Picard, L., Wlodawer, A., Lubkowski, J., and Kent, S. B. (1998) *Chem. Biol.* **6**, 43–51
 31. Lubkowski, J., Bujacz, G., Boque, L., Domaille, P. J., Handel, T. M., and Wlodawer, A. (1997) *Nat. Struct. Biol.* **4**, 64–69
 32. Malkowski, M. G., Wu, J. Y., Lazar, J. B., Johnson, P. H., and Edwards, B. F. P. (1995) *J. Biol. Chem.* **270**, 7077–7087
 33. Kao, J., Fan, Y. G., Haehnel, I., Brett, J., Greenberg, S., Clauss, M., Kayton, M., Houck, K., Kisiel, W., and Seljelid, R. (1994) *J. Biol. Chem.* **269**, 9774–9782
 34. Wakasugi, K., and Schimmel, P. (1999) *J. Biol. Chem.* **274**, 23155–23159
 35. Schimmel, P. (1995) *J. Mol. Evol.* **40**, 531–536
 36. Kim, S., Landro, J. A., Gale, A. J., and Schimmel, P. (1993) *Biochemistry* **32**, 13026–13031
 37. Whelihan, E. F., and Schimmel, P. (1997) *EMBO J.* **16**, 2968–2974